A&A 621, A16 (2019)
https://doi.org/10.1051/0004-6361/201833764

Astronomy & Astrophysics

Extended transition rates and lifetimes in Al I and Al II from systematic multiconfiguration calculations⋆

A. Papoulia (Ασημίνα Παπούλια)[1,2], J. Ekman[1], and P. Jönsson[1]

[1] Materials Science and Applied Mathematics, Malmö University, 20506 Malmö, Sweden
e-mail: asimina.papoulia@mau.se
[2] Division of Mathematical Physics, Lund University, Post Office Box 118, 22100 Lund, Sweden

Received 3 July 2018 / Accepted 22 September 2018

ABSTRACT

MultiConfiguration Dirac-Hartree-Fock (MCDHF) and relativistic configuration interaction (RCI) calculations were performed for 28 and 78 states in neutral and singly ionized aluminium, respectively. In Al I, the configurations of interest are $3s^2nl$ for $n = 3, 4, 5$ with $l = 0$ to 4, as well as $3s3p^2$ and $3s^26l$ for $l = 0, 1, 2$. In Al II, in addition to the ground configuration $3s^2$, the studied configurations are 3snl with $n = 3$ to 6 and $l = 0$ to 5, $3p^2$, 3s7s, 3s7p, and 3p3d. Valence and core-valence electron correlation effects are systematically accounted for through large configuration state function (CSF) expansions. Calculated excitation energies are found to be in excellent agreement with experimental data from the National Institute of Standards and Technology (NIST) database. Lifetimes and transition data for radiative electric dipole (E1) transitions are given and compared with results from previous calculations and available measurements for both Al I and Al II. The computed lifetimes of Al I are in very good agreement with the measured lifetimes in high-precision laser spectroscopy experiments. The present calculations provide a substantial amount of updated atomic data, including transition data in the infrared region. This is particularly important since the new generation of telescopes are designed for this region. There is a significant improvement in accuracy, in particular for the more complex system of neutral Al I. The complete tables of transition data are available at the CDS.

Key words. atomic data

1. Introduction

Aluminium is an important element in astrophysics. In newly born stars the galactic [Al/H] abundance ratio and the [Al/Mg] ratio are found to be increased in comparison to early stars (Clayton 2003). The aluminium abundance and its anti-correlation with that of magnesium is the best tool to determine which generation a globular cluster star belongs to. The abundance variations of different elements and the relative numbers of first- and second-generation stars can be used to determine the nature of polluting stars, the timescale of the star formation episodes, and the initial mass function of the stellar cluster (Carretta et al. 2010). The aluminium abundance is of importance for other types and groups of stars as well. A large number of spectral lines of neutral and singly ionized aluminium are observed in the solar spectrum and in many stellar spectra. Aluminium is one of the interesting elements for chemical analysis of the Milky Way, and one example is the *Gaia*-ESO Survey[1]; medium- and high-resolution spectra from more than 10^5 stars are analysed to provide public catalogues with astrophysical parameters. As part of this survey, Smiljanic et al. (2014) analysed high-resolution UVES[2] spectra of FGK-type stars and derived abundances for 24 elements, including aluminium.

In addition, aluminium abundances have been determined in local disk and halo stars by Gehren et al. (2004), Reddy et al. (2006), Mishenina et al. (2008), Adibekyan et al. (2012), and Bensby et al. (2014). However, chemical evolution models still have problems reproducing the observed behaviour of the aluminium abundance in relation to abundances of other elements. Such examples are the observed trends of the aluminium abundances in relation to metallicity [Fe/H], which are not well reproduced at the surfaces of stars, for example giants and dwarfs (Smiljanic et al. 2016). In light of the above issues, Smiljanic et al. (2016) redetermined aluminium abundances within the *Gaia*-ESO Survey. Furthermore, strong deviations from local thermodynamic equilibrium (LTE) are found to significantly affect the inferred aluminium abundances in metal poor stars, which was highlighted in the work by Gehren et al. (2006). Nordlander & Lind (2017) presented a non-local thermodynamic equilibrium (NLTE) modelling of aluminium and provided abundance corrections for lines in the optical and near-infrared regions.

Correct deduction of aluminium abundances and chemical evolution modelling is thus necessary to put together a complete picture of the stellar and Galactic evolution. Obtaining the spectroscopic reference data to achieve this goal is demanding. A significant amount of experimental research has been conducted to probe the spectra of Al II and Al I and to facilitate the analysis of the astrophysical observations. Even so, some laboratory measurements still lack reliability and in many cases, especially when going to higher excitation energies, only theoretical values of transition properties exist. Accurate computed atomic data are

⋆ The data are only available available at the CDS via anonymous ftp to cdsarc.u-strasbg.fr (130.79.128.5) or via http://cdsarc.u-strasbg.fr/viz-bin/qcat?J/A+A/621/A16

[1] http://casu.ast.cam.ac.uk/surveys-projects/ges

[2] http://www.eso.org/sci/facilities/paranal/instruments/uves.html

therefore essential to make abundance analyses in the Sun and other stars possible.

For the singly ionized Al II, there are a number of measurements of transition properties. The radiative lifetime of the $3s3p\ ^3P^o_1$ level was measured by Johnson et al. (1986) using an ion storage technique and the transition rate value for the inter-combination $3s3p\ ^3P^o_1 \rightarrow 3s^2\ ^1S_0$ transition was provided. Träbert et al. (1999) measured lifetimes in an ion storage ring and the result for the lifetime of the $3s3p\ ^3P^o_1$ level is in excellent agreement with the value measured by Johnson et al. (1986). Using the beam-foil technique, Andersen et al. (1971) measured lifetimes for the $3snf\ ^3F$ series with $n = 4-7$, although these measurements are associated with significant uncertainties. By using the same technique, the lifetime of the singlet $3s3p\ ^1P^o_1$ level was measured in four different experimental works (Kernahan et al. 1979; Head et al. 1976; Berry et al. 1970; Smith 1970), which are in very good agreement.

In the case of neutral Al I, several measurements have also been performed. Following a sequence of earlier works (Jönsson & Lundberg 1983; Jönsson et al. 1984), Buurman et al. (1986) used laser spectroscopy to obtain experimental values for the oscillator strengths of the lowest part of the spectrum. A few years later, Buurman & Dönszelmann (1990) redetermined the lifetime of the $3s^24p\ ^2P$ level and separated the different fine-structure components. Using similar laser techniques, Davidson et al. (1990) measured the natural lifetimes of the $3s^2nd\ ^2D$ Rydberg series and obtained oscillator strengths for transitions to the ground state. In a more recent work, Vujnović et al. (2002) used the hollow cathode discharge method to measure relative intensities of spectral lines of both neutral and singly ionized aluminium. Absolute transition probabilities were evaluated based on available results from previous studies, such as the ones mentioned above.

Al II is a nominal two-electron system and the lower part of its spectrum is strongly influenced by the interaction between the $3s3d\ ^1D$ and $3p^2\ ^1D$ configuration states. Contrary to neutral Mg I where no level is classified as $3p^2\ ^1D$, in Al II the $3p^2$ configuration dominates the lowest ^1D term and yields a well-localized state below the $3s3d\ ^1D$ term. The interactions between the $3snd\ ^1D$ Rydberg series and the $3p^2\ ^1D$ perturber were investigated by Tayal & Hibbert (1984). Going slightly further up, the spectrum of Al II is governed by the strong mixing of the $3snf\ ^3F$ Rydberg series with the $3p3d\ ^3F$ term. Despite the widespread mixing, $3p3d\ ^3F$ is also localized, between the $3s6f\ ^3F$ and $3s7f\ ^3F$ states. The configuration interaction between doubly excited states (e.g. the $3p^2\ ^1D$ and $3p3d\ ^3F$ states) and singly excited $3snl\ ^{1,3}L$ states was thoroughly investigated by Chang & Wang (1987). However, the extreme mixing of the $3p3d\ ^3F$ term in the $3snf\ ^3F$ series and its effect on the computation of transition properties was first investigated by Weiss (1974). Although the work by Chang & Wang (1987) was more of a qualitative nature, computed transition data were provided based on configuration interaction (CI) calculations. Using the B-spline configuration interaction (BSCI) method, Chang & Fang (1995) also predicted transition properties and lifetimes of Al II excited states.

Despite the large number of measured spectral lines in Al I, the $3s3p^2\ ^2D$ state could not be experimentally identified and for a long time theoretical calculations had been trying to localize it and predict whether it lies above or below the first-ionization limit. Al I is a system with three valence electrons, and the correlation effects are even stronger than in the singly ionized Al II. Especially strong is the two-electron interaction of $3s3d\ ^1D$ with $3p^2\ ^1D$, which becomes evident between the $3s^23d\ ^2D$ and $3s3p^2\ ^2D$ states. The $3s3p^2\ ^2D$ state is strongly coupled to the $3s^23d\ ^2D$ state, but it is also smeared out over the entire discrete part of the $3s^2nd\ ^2D$ series and contributes to a significant mixing of all those states (Weiss 1974). Asking for the position of the $3s3p^2\ ^2D$ level is thus meaningless since it does not correspond to any single spectral line (Lin 1974; Trefftz 1988). Due to this strong two-electron interaction, the line strength of one of the ^2D states involved in a transition appears to be enhanced, while the line strength of the other ^2D state is suppressed. This makes the computation of transition properties in Al I far from trivial (Froese Fischer et al. 2006). More theoretical studies on the system of neutral aluminium were conducted by Taylor et al. (1988) and Theodosiou (1992).

In view of the great astrophysical interest for accurate atomic data, close coupling (CC) calculations were carried out for the systems of Al II and Al I by Butler et al. (1993) and Mendoza et al. (1995), respectively, as part of the Opacity Project. These extended spectrum calculations produced transition data in the infrared region (IR), which had been scarce until then. However, the neglected relativistic effects and the insufficient amount of correlation included in the calculations constitute limiting factors to the accuracy of the results. Later on, Froese Fischer et al. (2006) performed MultiConfiguration Hartree-Fock (MCHF) calculations and used the Breit-Pauli (BP) approximation to also capture relativistic effects for Mg- and Al-like sequences. Focusing more on correlation, relativistic effects were kept to lower order. Even so, in Al I, correlation in the core and core-valence effects were not included due to limited computational resources. The latest compilation of Al II and Al I transition probabilities was made available by Kelleher & Podobedova (2008a). Wiese & Martin (1980) had earlier updated the first critical compilation of atomic data by Wiese et al. (1969).

Although for the past decades a considerable amount of research has been conducted for the systems of Al II and Al I, there is still a need for extended and accurate theoretical transition data. The present study is motivated by such a need. To obtain energy separations and transition data, the fully relativistic MultiConfiguration Dirac-Hartree-Fock (MCDHF) scheme has been employed. Valence and core-valence electron correlation is included in the computations of both systems. Spectrum calculations have been performed to include the first 28 and 78 lowest states in neutral and singly ionized aluminium, respectively. Transition data corresponding to IR lines have also been produced. The excellent description of energy separations is an indication of highly accurate computed atomic properties, which can be used to improve the interpretation of abundances in stars.

2. Theory

2.1. MultiConfiguration Dirac-Hartree-Fock approach

The wave functions describing the states of the atom, referred to as atomic state functions (ASFs), are obtained by applying the MCDHF approach (Grant 2007; Froese Fischer et al. 2016). In the MCDHF method, the ASFs are approximate eigenfunctions of the Dirac-Coulomb Hamiltonian given by

$$H_{DC} = \sum_{i=1}^{N}[c\ \boldsymbol{\alpha}_i \cdot \mathbf{p}_i + (\beta_i - 1)c^2 + V_{\rm nuc}(r_i)] + \sum_{i<j}^{N}\frac{1}{r_{ij}}, \quad (1)$$

where $V_{\rm nuc}(r_i)$ is the potential from an extended nuclear charge distribution, $\boldsymbol{\alpha}$ and β are the 4×4 Dirac matrices, c the speed of light in atomic units, and $\mathbf{p} \equiv -i\nabla$ the electron momentum

operator. An ASF $\Psi(\gamma PJM_J)$ is given as an expansion over $N_{\rm CSF}$ configuration state functions (CSFs), $\Phi(\gamma_i PJM_J)$, characterized by total angular momentum J and parity P:

$$\Psi(\gamma PJM_J) = \sum_{i=1}^{N_{\rm CSF}} c_i \Phi(\gamma_i PJM_J). \quad (2)$$

The CSFs are anti-symmetrized many-electron functions built from products of one-electron Dirac orbitals and are eigenfunctions of the parity operator P, the total angular momentum operator J^2 and its projection on the z-axis J_z (Grant 2007; Froese Fischer et al. 2016). In the expression above, γ_i represents the configuration, coupling, and other quantum numbers necessary to uniquely describe the CSFs.

The radial parts of the Dirac orbitals together with the mixing coefficients c_i are obtained in a self-consistent field (SCF) procedure. The set of SCF equations to be iteratively solved results from applying the variational principle on a weighted energy functional of all the studied states according to the extended optimal level (EOL) scheme (Dyall et al. 1989). The angular integrations needed for the construction of the energy functional are based on the second quantization method in the coupled tensorial form (Gaigalas et al. 1997, 2001).

The transverse photon (Breit) interaction and the leading quantum electrodynamic (QED) corrections (vacuum polarization and self-energy) can be accounted for in subsequent relativistic configuration interaction (RCI) calculations (McKenzie et al. 1980). In the RCI calculations, the Dirac orbitals from the previous step are fixed and only the mixing coefficients of the CSFs are determined by diagonalizing the Hamiltonian matrix. All calculations were performed using the relativistic atomic structure package GRASP2K (Jönsson et al. 2013).

In the MCDHF relativistic calculations, the wave functions are expansions over jj-coupled CSFs. To identify the computed states and adapt the labelling conventions followed by the experimentalists, the ASFs are transformed from jj-coupling to a basis of LSJ-coupled CSFs. In the GRASP2K code this is done using the methods developed by Gaigalas et al. (2003, 2004, 2017).

2.2. Transition parameters

In addition to excitation energies, lifetimes τ and transition parameters, such as emission transition rates A and weighted oscillator strengths gf, were also computed. The transition parameters between two states $\gamma' P' J'$ and γPJ are expressed in terms of reduced matrix elements of the transition operator $\mathbf{T}$ (Grant 1974):

$$\langle \Psi(\gamma PJ) \| \mathbf{T} \| \Psi(\gamma' P' J') \rangle = \sum_{k,l} c_k c'_l \langle \Phi(\gamma_k PJ) \| \mathbf{T} \| \Phi(\gamma'_l P' J') \rangle. \quad (3)$$

For electric multipole transitions, there are two forms of the transition operator: the length, which in fully relativistic calculations is equivalent to the Babushkin gauge, and the velocity form, which is equivalent to the Coulomb gauge. The transitions are governed by the outer part of the wave functions. The length form is more sensitive to this part of the wave functions and it is generally considered to be the preferred form. Regardless, the agreement between the values of these two different forms can be used to indicate the accuracy of the wave functions (Froese Fischer 2009; Ekman et al. 2014). This is particularly useful when no experimental measurements are available. The transitions can be organized in groups determined, for instance, by the magnitude of the transition rate value. A statistical analysis of the uncertainties of the transitions can then be performed. For each group of transitions the average uncertainty of the length form of the computed transition rates is given by

$$\langle \mathrm{d}T \rangle = \frac{1}{N} \sum_{i=1}^{N} \frac{|A_l^i - A_v^i|}{\max(A_l^i, A_v^i)}, \quad (4)$$

where A_l and A_v are respectively the transition rates in length and velocity form for a transition i and N is the number of the transitions belonging to a group. In this work, we only computed transition parameters for the electric dipole (E1) transitions. The electric quadrupole (E2) and magnetic multipole (Mk) transitions are much weaker and therefore less likely to be observed.

3. Calculations

3.1. Al I

In neutral aluminium, calculations were performed in the EOL scheme (Dyall et al. 1989) for 28 targeted states. These states belong to the $3s^2ns$ configurations with $n = 4, 5, 6$, the $3s^2nd$ configurations with $n = 3, ..., 6$, and the $3s3p^2$ and $3s^25g$ configurations, characterized by even parity, and on the other hand the $3s^2np$ configurations with $n = 3, .., 6$ and the $3s^24f$ and $3s^25f$ configurations, characterized by odd parity. These configurations define what is known as the multireference (MR). From initial calculations and analysis of the eigenvector compositions, we deduced that all $3p^2nl$ configurations, in addition to the targeted $3s^2nl$, give considerable contributions to the total wave functions and should be included in the MR. Following the active set (AS) approach (Olsen et al. 1988; Sturesson et al. 2007), the CSF expansions (see Eq. (2)) were obtained by allowing single and restricted double (SD) substitutions of electrons from the reference (MR) orbitals to an AS of correlation orbitals. The AS is systematically increased by adding layers of orbitals to effectively build nearly complete wave functions. This is achieved by keeping track of the convergence of the computed excitation energies, and of the other physical quantities of interest, such as the transition parameters here.

As a first step an MCDHF calculation was performed for the orbitals that are part of the MR. States with both even and odd parity were simultaneously optimized. Following this step, we continued to optimize six layers of correlation orbitals based on valence (VV) substitutions. The VV expansions were obtained by allowing SD substitutions from the three outer valence orbitals in the MR, with the restriction that there will be at most one substitution from orbitals with $n = 3$. In this manner, the correlation orbitals will occupy the space between the inner $n = 3$ valence orbitals and the outer orbitals involved in the higher Rydberg states (see Fig. 1). These orbitals have been shown to be of crucial importance for the transition probabilities, which are weighted towards this part of the space (Pehlivan Rhodin et al. 2017; Pehlivan Rhodin 2018). The six correlation layers correspond to the 12s, 12p, 12d, 11f, 11g, and 10h set of orbitals.

Each MCDHF calculation was followed by an RCI calculation for an extended expansion, obtained by single, double, and triple (SDT) substitutions from the valence orbitals. As a final step, an RCI calculation was performed for the largest SDT valence expansion augmented by a core-valence (CV) expansion. The CV expansion was obtained by allowing SD substitutions from the valence orbitals and the $2p^6$ core, with the restriction that there will be at most one substitution from

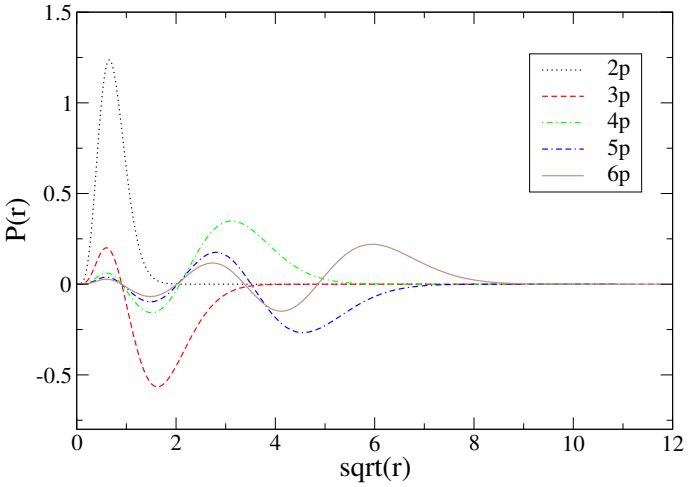

Fig. 1. Al I Dirac-Fock radial orbitals for the p symmetry, as a function of $\sqrt{r}$. The 2p orbital is part of the core and the orbitals from $n = 3$ to $n = 6$ are part of the valence electron cloud. These orbitals occupy different regions in space and the overlap between some of the Rydberg states is minor.

$2p^6$. All the RCI calculations included the Breit interaction and the leading QED effects. Accounting for CV correlation does not lower the total energies significantly, but it can have large effects on the energy separations and thus we considered it crucial. Core-valence correlation is also important for transition properties (Hibbert 1989). Core-core (CC) correlation, obtained by allowing double excitations from the core, is known to be less important and has not been considered in the present work. The number of CSFs in the final even and odd state expansions, accounting for both VV and CV electron correlation, were 4 362 628 and 2 889 385, respectively, distributed over the different J symmetries.

3.2. Al II

In the singly ionized aluminium, the calculations were more extended, including 78 targeted states. These states belong to the $3s^2$ ground configuration, and to the $3p^2$; the 3sns configurations with $n = 4, ..., 7$; the 3snd with $n = 3, ..., 6$; and the 3s5g and 3s6g configurations, characterized by even parity, and on the other hand, the 3snp configurations with $n = 3, ..., 7$; the 3snf with $n = 4, 5, 6$; and the 3s6h and 3p3d configurations, characterized by odd parity. These configurations define the multireference (MR). In the computations of Al II, the EOL scheme was applied and the CSF expansions were obtained following the active set (AS) approach, accounting for VV and CV correlation. Al II is less complex and the CSF expansions generated from (SD) substitutions are not as large as those in Al I. Hence, we can afford both 2s and 2p orbitals to account for CV correlation. The 1s core orbital remained closed and, as it was for Al I, core-core correlation was neglected. The MCDHF calculations were performed in a similar way to the calculations in Al I, yet no particular restrictions were imposed on the VV substitutions. We optimized six correlation layers corresponding to the 13s, 13p, 12d, 12f, 12g, 8h, and 7i set of orbitals. Each MCDHF calculation was followed by an RCI calculation. Finally, an RCI calculation was performed for the largest SD valence expansion augmented by the CV expansion. The number of CSFs in the final even and odd state expansions, accounting for both VV and CV electron correlation, were 911 795 and 1 269 797, respectively, distributed over the different J symmetries.

4. Results

4.1. Al I

In Table 1 the computed excitation energies, based on VV correlation, are given as a function of the increasing active set of orbitals. After adding the $n = 11$ correlation layer, we note that the energy values for all 28 targeted states have converged. For comparison, in the second last column the observed energies from the National Institute of Standards and Technology (NIST) Atomic Spectra Database (Kramida et al. 2018) are displayed. All energies but those belonging to the $3s3p^2$ configuration are already in good agreement with the NIST recommended values. The relative differences between theory and experiment for all three levels of the quartet $3s3p^2\ ^4P$ state is 3.1%, while the mean relative difference for the rest of the states is less than 0.2%. In the third last column, the computed excitation energies after accounting for CV correlation are displayed. When taking into account CV effects the agreement with the observed values is better overall. Most importantly, for the $3s3p^2\ ^4P$ levels the relative differences between observed and computed values decrease to less than 0.6%. The likelihood that the $1s^22s^22p^6$ core overlaps with the $3s3p^2$ cloud of electrons is much less than that for $3s^2nl$. Consequently, when CV correlation is taken into account the lowering of the $3s3p^2$ energy levels is much smaller than for levels belonging to any $3s^2nl$ configuration. Thus, the adjustments to the separation energies will be minor between the ground state $3s^23p$ and $3s^2nl$ levels, but significant between the $3s^23p$ and $3s3p^2$ levels. In the last column of Table 1 the differences $\Delta E = E_{\rm obs} - E_{\rm theor}$, between the final (CV) computed and the observed energies, are also displayed. In principle, there are two groups of values; the one consisting of the $3s^2nd$ configurations exhibits the smallest absolute discrepancies from the observed energies. For the rest, the absolute discrepancies are somewhat larger.

In the calculations, the labelling of the eigenstates is determined by the CSF with the largest coefficient in the expansion of Eq. (2). When the same label is assigned to different eigenstates, a detailed analysis can be performed by displaying their LS-compositions. In Table 1, we note that two of the states have been assigned the same label, i.e. $3s^24d\ ^2D$, and thus the subscripts a and b are used to distinguish them. In Table 2, we give the LS-composition of all computed $3s^2nd\ ^2D$ states, including the three most dominant CSFs. The $3s^24d\ ^2D$ term appears twice as the CSF with the largest LS-composition. Moreover, the admixture of the $3s3p^2\ ^2D$ in the four lowest $3s^2nd\ ^2D$ states is rather strong and adds up to 65%. That being so, the $3s3p^2\ ^2D$ does not exist in the calculated spectrum as a localized state. For comparison, in the last column of Table 2 the labelling of the observed $3s^2nd\ ^2D$ states is also given. In the observed configurations presented by NIST (Kramida et al. 2018), the second highest $3s^2nd\ ^2D$ term has not been given any specific label and it is therefore designated as $y\ ^2D$. The higher ^2D terms are designated as $3s^24d$, $3s^25d$, and so on.

In Table 3, the current results for the lowest excitation energies are compared with the values from the MCHF-BP calculations by Froese Fischer et al. (2006). The latter calculations are extended up to levels corresponding to the doublet $3s^24p\ ^2P$ state. The differences ΔE between observed and computed energies are given in the last two columns for the different computational approaches. As can be seen, when using the current MCDHF and RCI method the agreement with the observed energies is substantially improved for all levels and in particular, for those belonging to the quartet $3s3p^2\ ^4P$ state. In the MCHF-BP calculations, core-valence correlation was neglected. As

Table 1. Computed excitation energies in cm^{-1} for the 28 lowest states in Al I.

			VV								
Pos.	Conf.	*LS J*	$n = 7$	$n = 8$	$n = 9$	$n = 10$	$n = 11$	$n = 12$	CV	E_{obs}[a]	ΔE
1	$3s^2\,3p$	$^2P^o_{1/2}$	0	0	0	0	0	0	0	0	0
2		$^2P^o_{3/2}$	108	108	108	108	108	108	104	112	8
3	$3s^2\,4s$	$^2S_{1/2}$	25 318	25 377	25 416	25 419	25 427	25 429	25 196	25 348	152
4	$3s\,3p^2$	$^4P_{1/2}$	27 788	27 966	28 073	28 085	28 109	28 111	28 863	29 020	157
5		$^4P_{3/2}$	27 833	28 011	28 118	28 130	28 154	28 156	28 907	29 067	160
6		$^4P_{5/2}$	27 906	28 085	28 191	28 204	28 227	28 230	28 981	29 143	162
7	$3s^2\,3d$	$^2D_{3/2}$	32 211	32 077	32 135	32 139	32 150	32 150	32 414	32 435	21
8		$^2D_{5/2}$	32 212	32 079	32 137	32 141	32 152	32 152	32 416	32 437	21
9	$3s^2\,4p$	$^2P^o_{1/2}$	32 770	32 879	32 935	32 937	32 946	32 949	32 801	32 950	149
10		$^2P^o_{3/2}$	32 786	32 894	32 951	32 952	32 962	32 964	32 814	32 966	152
11	$3s^2\,5s$	$^2S_{1/2}$	37 493	37 637	37 693	37 694	37 704	37 706	37 512	37 689	177
12	$3s^2\,4d$	$^2D_{3/2\,a}$	38 733	38 659	38 711	38 707	38 717	38 718	38 951	38 929	−22
13		$^2D_{5/2\,a}$	38 736	38 664	38 717	38 712	38 722	38 724	38 957	38 934	−23
14	$3s^2\,5p$	$^2P^o_{1/2}$	40 038	40 187	40 252	40 249	40 259	40 262	40 101	40 272	171
15		$^2P^o_{3/2}$	40 043	40 193	40 258	40 255	40 265	40 268	40 106	40 278	172
16	$3s^2\,4f$	$^2F^o_{5/2}$	41 050	41 209	41 282	41 287	41 297	41 300	41 163	41 319	156
17		$^2F^o_{7/2}$	41 050	41 209	41 282	41 287	41 297	41 300	41 163	41 319	156
18	$3s^2\,6s$	$^2S_{1/2}$	41 897	42 069	42 133	42 135	42 144	42 143	41 964	42 144	180
19	$3s^2\,4d$	$^2D_{3/2\,b}$	42 105	42 071	42 121	42 108	42 119	42 121	42 232	42 234	2
20		$^2D_{5/2\,b}$	42 109	42 075	42 126	42 112	42 123	42 125	42 237	42 238	1
21	$3s^2\,6p$	$^2P^o_{1/2}$	43 076	43 246	43 316	43 311	43 321	43 324	43 160	43 335	175
22		$^2P^o_{3/2}$	43 079	43 249	43 318	43 313	43 324	43 326	43 162	43 338	176
23	$3s^2\,5f$	$^2F^o_{5/2}$	43 549	43 721	43 795	43 801	43 811	43 813	43 660	43 831	171
24		$^2F^o_{7/2}$	43 549	43 721	43 795	43 801	43 811	43 813	43 660	43 831	171
25	$3s^2\,5g$	$^2G_{7/2}$	43 576	43 763	43 838	43 845	43 856	43 859	43 687	43 876	189
26		$^2G_{9/2}$	43 576	43 763	43 838	43 845	43 856	43 859	43 687	43 876	189
27	$3s^2\,5d$	$^2D_{3/2}$	44 034	44 059	44 115	44 096	44 106	44 109	44 126	44 166	40
28		$^2D_{5/2}$	44 036	44 062	44 117	44 099	44 109	44 111	44 129	44 169	40

Notes. The energies are given as a function of the increasing active set of orbitals, accounting for VV correlation, where n indicates the maximum principle quantum number of the orbitals included in the active set. In Col. 10, the final energy values are displayed after accounting for CV correlation. The differences ΔE between the final computations and the observed values are shown in the last column. The sequence and labelling of the configurations and *LS J*-levels are in accordance with the final (CV) computed energies. The $3s^24d\ ^2D$ term is assigned twice throughout the calculations (see also Table 2) and the subscripts *a* and *b* are used to distinguish them. See text for details.
References. [(a)]NIST Atomic Spectra Database 2018 (Kramida et al. 2018).

Table 2. *LS*-composition of the computed states belonging to the strongly mixed $3s^2$nd Rydberg series in Al I.

Pos.	Conf.	*LS J*	*LS*-composition	Label used in NIST[(1)]
7,8	$3s^2\,3d$	$^2D_{3/2,5/2}$	0.67 + 0.19 $3s\,3p^2\ ^2D$ + 0.04 $3s^2\,4d\ ^2D$	$3s^2\,3d\ ^2D_{3/2,5/2}$
12,13	$3s^2\,4d$	$^2D_{3/2,5/2\,a}$	0.41 + 0.22 $3s^2\,3d\ ^2D$ + 0.21 $3s\,3p^2\ ^2D$	$3s^2$ nd y $^2D_{3/2,5/2}$
19,20	$3s^2\,4d$	$^2D_{3/2,5/2\,b}$	0.44 + 0.25 $3s^2\,5d\ ^2D$ + 0.15 $3s\,3p^2\ ^2D$	$3s^2\,4d\ ^2D_{3/2,5/2}$
27,28	$3s^2\,5d$	$^2D_{3/2,5/2}$	0.58 + 0.19 $3s^2\,6d\ ^2D$ + 0.10 $3s\,3p^2\ ^2D$	$3s^2\,5d\ ^2D_{3/2,5/2}$

Notes. The three most dominant *LS*-components are displayed. The first percentage value corresponds to the assigned configuration and term. In all these cases, the percentages for the two different *LS J*-levels are the same and are therefore given in the same line. In the last column we provide the labelling of the corresponding observed terms as given in the NIST Database. The first column refers to the positions according to Table 1.
References. [(1)]Kramida et al. (2018).

mentioned above and also acknowledged by Froese Fischer et al. (2006), capturing such correlation effects is crucial for 3s-hole states, such as states with significant $3s3p^2$ composition. Furthermore, the $\Delta E_{MCHF-BP}$ values do not always have the same sign, while the ΔE_{RCI} differences are consistently positive. This is particularly important when calculating transition properties. On average, properties for transitions between two levels for which the differences $\Delta E_{MCHF-BP}$ have opposite signs are estimated less accurately.

The complete transition data tables, for all computed E1 transitions in Al I, can be found at the CDS. In the CDS table, the transition energies, wavelengths and the length form of the

Table 3. Observed and computed excitation energies in cm^{-1} for the 10 and 20 lowest states in Al I and Al II, respectively.

Pos.	Conf.	$LS\,J$	E_{obs}[a]	E_{RCI}[b]	ΔE_{RCI}[b]	$\Delta E_{MCHF-BP}$[c]
			Al I			
1	$3s^2\,3p$	$^2P^o_{1/2}$	0	0	0	0
2		$^2P^o_{3/2}$	112	104	8	22
3	$3s^2\,4s$	$^2S_{1/2}$	25 348	25 196	152	−235
4	$3s\,3p^2$	$^4P_{1/2}$	29 020	28 863	157	940
5		$^4P_{3/2}$	29 067	28 907	160	949
6		$^4P_{5/2}$	29 143	28 981	162	964
7	$3s^2\,3d$	$^2D_{3/2}$	32 435	32 414	21	250
8		$^2D_{5/2}$	32 437	32 416	21	251
9	$3s^2\,4p$	$^2P^o_{1/2}$	32 950	32 801	149	−98
10		$^2P^o_{3/2}$	32 966	32 814	152	−94
			Al II			
1	$3s^2$	$^1S_0$	0	0	0	0
2	$3s\,3p$	$^3P^o_0$	37 393	37 445	−52	9
3		$^3P^o_1$	37 454	37 503	−49	8
4		$^3P^o_2$	37 578	37 626	−48	6
5		$^1P^o_1$	59 852	59 982	−130	−177
6	$3p^2$	$^1D_2$	85 481	85 692	−211	−305
7	$3s\,4s$	$^3S_1$	91 275	91 425	−150	−376
8	$3p^2$	$^3P_0$	94 085	94 211	−126	−107
9		$^3P_1$	94 147	94 264	−117	−111
10		$^3P_2$	94 269	94 375	−106	−113
11	$3s\,4s$	$^1S_0$	95 351	95 543	−192	−400
12	$3s\,3d$	$^3D_2$	95 549	95 791	−242	−527
13		$^3D_1$	95 551	95 794	−243	−527
14		$^3D_3$	95 551	95 804	−253	−529
15	$3s\,4p$	$^3P^o_0$	105 428	105 582	−154	−357
16		$^3P^o_1$	105 442	105 594	−152	−360
17		$^3P^o_2$	105 471	105 623	−152	−363
18		$^1P^o_1$	106 921	107 132	−211	−365
19	$3s\,3d$	$^1D_2$	110 090	110 330	−240	−475
20	$3p^2$	$^1S_0$	111 637	112 086	−449	−445

Notes. In the last two columns, the difference ΔE between observed and computed energies is compared for the current RCI and previous MCHF-BP calculations.
References. [(a)]Kramida et al. (2018); [(b)]present calculations; [(c)]Froese Fischer et al. (2006).

Table 4. Statistical analysis of the uncertainties of the computed transition rates in Al I and Al II.

	A^{low}_{RCI}	A^{high}_{RCI}	No.Trans.	$\langle dT\rangle$	Q_3	Max
			Al I			
1		1.00E+05	31	0.62	0.83	0.98
2	1.00E+05	1.00E+06	25	0.29	0.37	0.81
3	1.00E+06	1.00E+07	24	0.055	0.076	0.15
4	1.00E+07		20	0.043	0.073	0.14
			Al II			
1		1.00E+05	109	0.07	0.11	0.61
2	1.00E+05	1.00E+06	81	0.09	0.11	0.67
3	1.00E+06	1.00E+07	99	0.043	0.036	0.39
4	1.00E+07		141	0.011	0.009	0.12

Notes. The transition rates are arranged in four groups and in Col. 4, the number of transitions belonging to each group is given. In the last three columns, the average value, the value Q_3 containing 75% of the lowest computed dT values, and the maximum value are given for each group of transitions. All transition rates are given in s^{-1}.

transition rates A, and weighted oscillator strengths gf are given. Based on the agreement between the length and velocity forms of the computed transition rates A_{RCI}, a statistical analysis of the uncertainties can be preformed. The transitions were arranged in four groups based on the magnitude of the A_{RCI} values. The first two groups contain all the weak transitions with transition rates up to $A = 10^6\ s^{-1}$, while the next two groups contain the strong transitions with $A > 10^6\ s^{-1}$. In Table 4, the average value of the uncertainties $\langle dT\rangle$ (see Eq. (4)) is given for each group of transitions. To better understand how the individual uncertainties dT are distributed, the maximum value and the value Q_3 containing 75% of the lowest computed dT values (third quartile) are also given in Table 4. When examining the predicted uncertainties of the individual groups, we deduce that for all the strong transitions dT always remains below 15%. Most of the strong transitions are associated with small uncertainties, which justifies the low average values. Contrary to the strong transitions, the weaker transitions are associated with considerably larger uncertainties. This is even more pronounced for the first group of transitions where A is less than $10^5\ s^{-1}$. The weak E1 transitions are challenging, and therefore interesting, from a theoretical point

Table 5. Comparison between computed and observed transition rates A in s^{-1} for selected transitions in Al I.

Upper	Lower	A_{RCI}[a]	$A_{MCHF-BP}$[b]	A_{CC}[c]	A_{obs}[d,e,f]	A_{obs}[g]
$3s^2\,4s\ ^2S_{1/2}$	$3s^2\,3p\ ^2P^o_{1/2}$	4.966E+07	5.098E+07		4.93E+07[d C]	4.70E+07[B]
	$3s^2\,3p\ ^2P^o_{3/2}$	9.884E+07	10.15E+07		9.80E+07[d C]	9.90E+07[B]
$3s^2\,5s\ ^2S_{1/2}$	$3s^2\,3p\ ^2P^o_{1/2}$	1.277E+07			1.33E+07[d C]	1.42E+07[C+]
	$3s^2\,3p\ ^2P^o_{3/2}$	2.534E+07			2.64E+07[d C]	2.84E+07[C+]
$3s^2\,5s\ ^2S_{1/2}$	$3s^2\,4p\ ^2P^o_{1/2}$	3.815E+06				3.00E+06[D]
	$3s^2\,4p\ ^2P^o_{3/2}$	7.599E+06				6.00E+06[D]
$3s^2\,4p\ ^2P^o_{1/2}$	$3s^2\,4s\ ^2S_{1/2}$	1.580E+07	1.507E+07		1.69E+07[e C+]	1.60E+07[A]
$3s^2\,4p\ ^2P^o_{3/2}$	$3s^2\,4s\ ^2S_{1/2}$	1.587E+07	1.514E+07		1.69E+07[e C+]	1.50E+07[B]
$3s^2\,3d\ ^2D_{3/2}$	$3s^2\,3p\ ^2P^o_{1/2}$	6.542E+07	5.651E+07		6.30E+07[d C]	5.90E+07[C+]
	$3s^2\,3p\ ^2P^o_{3/2}$	1.321E+07	1.140E+07			(1.20)E+07
$3s^2\,3d\ ^2D_{5/2}$	$3s^2\,3p\ ^2P^o_{3/2}$	7.877E+07	6.806E+07		7.40E+07[d C]	7.10E+07[A]
$3s^2\,4d\ ^2D_{3/2\ a}$	$3s^2\,3p\ ^2P^o_{1/2}$	1.722E+07			1.92E+07[f C+]	
					2.30E+07[d C]	
	$3s^2\,3p\ ^2P^o_{3/2}$	3.293E+06		5.99E+06	3.80E+06[f C+]	
					4.40E+06[d C]	
$3s^2\,4d\ ^2D_{5/2\ a}$	$3s^2\,3p\ ^2P^o_{3/2}$	2.010E+07		3.60E+07	2.30E+07[f]	
					2.80E+07[d C]	
$3s^2\,4d\ ^2D_{3/2\ b}$	$3s^2\,3p\ ^2P^o_{1/2}$	7.128E+07		7.61E+07	7.20E+07[d C]	
					5.26E+07[f]	
	$3s^2\,3p\ ^2P^o_{3/2}$	1.386E+07		1.51E+07	1.40E+07[d C]	
					1.05E+07[f A]	
$3s^2\,4d\ ^2D_{5/2\ b}$	$3s^2\,3p\ ^2P^o_{3/2}$	8.412E+07		9.07E+07	8.60E+07[d C]	
					6.31E+07[f]	
$3s^2\,5d\ ^2D_{3/2}$	$3s^2\,3p\ ^2P^o_{1/2}$	8.204E+07			6.60E+07[d C]	
					5.76E+07[f]	
	$3s^2\,3p\ ^2P^o_{3/2}$	1.596E+07		1.26E+07	1.30E+07[d C]	
					1.15E+07[f]	
$3s^2\,5d\ ^2D_{5/2}$	$3s^2\,3p\ ^2P^o_{3/2}$	9.706E+07		7.58E+07	7.90E+07[d C]	
					6.91E+07[f]	

Notes. The present values from the RCI calculations are given in Col. 3. In the next two columns, theoretical values from former MCHF-BP and close coupling (CC) calculations are displayed. The CC values complement the MCHF-BP values, which are restricted to transitions between levels in the lower part of the Al I spectrum. All theoretical transition rates are presented in length form. The last two columns contain the results from experimental observations. The experimental results go along with a letter grade, whenever accessible, which indicates the accuracy level. The correspondence between the accuracy ratings and the estimated relative uncertainty of the experimental results is $A \leq 3\%$, $B \leq 10\%$, $C+ \leq 15\%$, $C \leq 25\%$, $D+ \leq 30\%$, $D \leq 50\%$.

References. [(a)]Present calculations; [(b)]Froese Fischer et al. (2006); [(c)]Mendoza et al. (1995); [(d)]Wiese & Martin (1980); [(e)]Buurman et al. (1986); [(f)]Davidson et al. (1990); [(g)]Vujnović et al. (2002).

of view, although they are less likely to be observed. The computation of transition properties in the system of Al I is overall far from trivial due to the extreme mixing of the $3s^2nd\ ^2D$ series. Transitions involving any ^2D state as upper or lower level appear to be associated with large uncertainties. However, the predicted energy separations are in excellent agreement with observations, meaning that the LS-composition of the $3s^2nd\ ^2D$ states is well described. This should serve as a quality indicator of the computed transition data.

Transition rates A_{obs} evaluated from experimental measurements are compared with the current RCI theoretical values (see Table 5) and with values from the MCHF-BP calculations by Froese Fischer et al. (2006) and the close coupling (CC) calculations by Mendoza et al. (1995). Even though the measurements by Davidson et al. (1990) are more recent than the compiled values by Wiese & Martin (1980), the latter seem to be in better overall agreement with the transition rates predicted by the RCI calculations. In all cases the A_{RCI} values fall into the range of the estimated uncertainties by Wiese & Martin (1980). The only exceptions are the transitions with $3s^24d\ ^2D_{3/2,5/2\ a}$ as upper levels, for which the A_{RCI} values agree better with the ones suggested by Davidson et al. (1990). Although the evaluated transition rates by Vujnović et al. (2002) slightly differ from the other observations, they are still in fairly good agreement with the present work. For the $3s^24p\ ^2P^o_{3/2} \rightarrow 3s^24s\ ^2S_{1/2}$ and $3s^23d\ ^2D_{5/2} \rightarrow 3s^23p\ ^2P^o_{3/2}$ transitions, the values by Vujnović et al. (2002) are better reproduced by the $A_{MCHF-BP}$ results, yet not enough correlation is included in the calculations by Froese Fischer et al. (2006) and the transition rates predicted by the RCI calculations should be considered more accurate. Whenever values from the close coupling (CC) calculations are presented to complement the MCHF-BP

Table 6. Comparison between computed and observed lifetimes τ in seconds for the 26 lowest excited states in Al I.

			RCI[a]		MCHF-BP[b]	Expt.[c,d,e]
Pos.	Conf.	*LS J*	τ_l	τ_v	τ_l	$\tau_{\rm obs}$
1	$3s^2\,4s$	$^2S_{1/2}$	6.734E-09	6.745E-09	6.558E-09	6.85(6)E-09[c]
2	$3s\,3p^2$	$^4P_{1/2}$	1.652E-03	1.182E-03	4.950E-03	
3		$^4P_{3/2}$	6.702E-03	6.911E-03	13.24E-03	
4		$^4P_{5/2}$	2.604E-03	3.681E-03	9.486E-03	
5	$3s^2\,3d$	$^2D_{3/2}$	1.272E-08	1.372E-08	1.472E-08	1.40(2)E-08[c]
6		$^2D_{5/2}$	1.270E-08	1.371E-08	1.469E-08	1.40(2)E-08[c]
7	$3s^2\,4p$	$^2P^o_{1/2}$	6.329E-08	6.357E-08	6.621E-08	6.05(9)E-08[e]
8		$^2P^o_{3/2}$	6.300E-08	6.328E-08	6.590E-08	6.5 (2) E-08[e]
9	$3s^2\,5s$	$^2S_{1/2}$	2.019E-08	2.027E-08		1.98(5)E-08[c]
10	$3s^2\,4d$	$^2D_{3/2\,a}$	3.117E-08	2.919E-08		2.95(7)E-08[c]
11		$^2D_{5/2\,a}$	3.158E-08	2.953E-08		2.95(7)E-08[c]
12	$3s^2\,5p$	$^2P^o_{1/2}$	2.448E-07	2.532E-07		2.75(8)E-07[c]
13		$^2P^o_{3/2}$	2.429E-07	2.512E-07		2.75(8)E-07[c]
14	$3s^2\,4f$	$^2F^o_{5/2}$	6.041E-08	6.162E-08		
15		$^2F^o_{7/2}$	6.041E-08	6.160E-08		
16	$3s^2\,6s$	$^2S_{1/2}$	4.812E-08	4.885E-08		
17	$3s^2\,4d$	$^2D_{3/2\,b}$	1.136E-08	1.083E-08		1.32(3)E-08[d]
18		$^2D_{5/2\,b}$	1.150E-08	1.093E-08		1.32(3)E-08[d]
19	$3s^2\,6p$	$^2P^o_{1/2}$	4.886E-07	6.952E-07		
20		$^2P^o_{3/2}$	4.845E-07	6.882E-07		
21	$3s^2\,5f$	$^2F^o_{7/2}$	1.176E-07	1.172E-07		
22		$^2F^o_{5/2}$	1.175E-07	1.172E-07		
23	$3s^2\,5g$	$^2G_{7/2}$	2.301E-07	2.315E-07		
24		$^2G_{9/2}$	2.301E-07	2.315E-07		
25	$3s^2\,5d$	$^2D_{3/2}$	1.011E-08	9.855E-09		14.0(2)E-09[d]
26		$^2D_{5/2}$	1.020E-08	9.921E-09		14.0(2)E-09[d]

Notes. For the current RCI calculations both length τ_l and velocity τ_v forms are displayed. In Col. 6, the predicted lifetimes from MCHF-BP calculations are given in length form. The last column contains available lifetimes from experimental measurements together with their uncertainties.

References. [(a)]Present calculations; [(b)]Froese Fischer et al. (2006); [(c)]Buurman et al. (1986); [(d)]Davidson et al. (1990); [(e)]Buurman & Dönszelmann (1990).

results, the $A_{\rm RCI}$ values appear to be in better agreement with the experimental values. Exceptionally, for the $3s^25d\ ^2D_{3/2,5/2} \rightarrow 3s^23p\ ^2P^o_{3/2}$ transitions, the $A_{\rm CC}$ values by Mendoza et al. (1995) approach the corresponding experimental values more closely. Even so, the $A_{\rm RCI}$ values are still within the given experimental uncertainties. One should bear in mind that according to the estimation of uncertainties by Kelleher & Podobedova (2008b) the $A_{\rm CC}$ values carry relative uncertainties up to 30%. On the contrary, based on the agreement between length and velocity forms, the estimated uncertainties of the current RCI calculations for the above-mentioned transitions are of the order of 3% percent. Therefore, we suggest that the current transition rates are used as a reference.

From the computed E1 transition rates, the lifetimes of the excited states are estimated. Transition data for transitions other than E1 have not been computed in this work since the contributions to the lifetimes from magnetic or higher electric multipoles are expected to be negligible. In Table 6 the currently computed lifetimes are given in both length τ_l and velocity τ_v forms. The agreement between these two forms probes the level of accuracy of the calculations. Because of the poor agreement between the length and velocity form of the quartet $3s3p^2\ ^4P$ and doublet $3s^26p\ ^2P$ states, the average relative difference appears overall to be ~8%. The differences between the length and velocity gauges of the quartet $3s3p^2\ ^4P$ states are of the order of 25% on average. These long-lived states are associated with weak transitions and computations involving such transitions are, as mentioned above, rather challenging. In addition, we note that the relative differences corresponding to the $3s^26p\ ^2P$ states exceed 40%. As the computations involve Rydberg series, states between the lowest and highest computed levels might not occupy the same region in space. Nevertheless, these states are part of the same multireference (MR). The highest computed levels correspond to configurations with orbitals up to $n = 6$, such as $3s^26p$. To obtain a better description of these levels it is probably necessary to perform initial calculations including in the MR $3s^2nl$ configurations with $n = 7$ and perhaps even $n = 8$. This would lead to a more complete and balanced orbital set (Pehlivan Rhodin et al. 2017). When excluding the above-mentioned states, the mean relative difference between τ_l and τ_v is ~3%, which is satisfactory.

In Table 6, the lifetimes from the current RCI calculations are compared with results from the MCHF-BP calculations by Froese Fischer et al. (2006) and observations. Only for the $3s^24p\ ^2P$ state are separated observed values of the lifetimes given for the two fine-structure components. For the rest of the

measured lifetimes, a single value for the two fine-structure levels is provided. As can be seen, the overall agreement between the theoretical and the measured lifetimes $\tau_{\rm obs}$ is rather good. However, the measured lifetimes are better represented by the current RCI results than by the MCHF-BP values. For most of the states, the differences between the RCI and MCHF-BP values are small, except for the levels of the quartet $3s3p^2\ ^4P$ state. For these long-lived states, no experimental lifetimes exist for comparison.

4.2. Al II

In Table A.1, the computed excitation energies, based on VV correlation, are given as a function of the increasing active set of orbitals. When adding the $n = 12$ correlation layer, the values for all computed energy separations have converged. The agreement with the NIST observed energies (Kramida et al. 2018) is, at this point, fairly good. The mean relative difference between theory and experiment is of the order of 1.2%. However, when accounting for CV correlation, the agreement with the observed values is significantly improved, resulting in a mean relative difference being less than 0.2%. Accounting for CV effects also results in a labelling of the eigenstates that matches observations. For instance, when only VV correlation is taken into account, the ^{3}F triplet with the highest energy is labelled as a 3s6f level. After taking CV effects into account, the eigenstates of this triplet are assigned the 3p3d configuration, now the one with the largest expansion coefficient, which agrees with observations. There are no experimental excitation energies for the singlet and triplet 3s6h $^{1,3}H$ terms. In the last column of Table A.1, the differences ΔE between computed and observed energies are displayed. All ΔE values maintain the same sign, being negative.

In Table 3, a comparison between the present computed excitation energies and those from the MCHF-BP calculations by Froese Fischer et al. (2006) is also performed for Al II. The latter spectrum calculations are extended up to levels corresponding to the singlet $3p^2\ ^1$S state and all types of correlation, i.e. VV, CV, and CC, were accounted for. Both computational approaches are highly accurate, yet the majority of the levels is better represented by the current RCI results. The average relative difference for the RCI values is ∼0.2% and for the MCHF-BP ∼0.3%. Moreover, the $\Delta E_{\rm MCHF-BP}$ values do not always maintain the same sign, while the $\Delta E_{\rm RCI}$ values do. Hence, in general, the MCHF-BP calculations do not predict the transition energies as precisely as the present RCI method.

For all computed E1 transitions in Al II, transition data tables can also be found at the CDS. In Table 4, a statistical analysis of the uncertainties to the computed transition rates $A_{\rm RCI}$ is performed in a similar way to that for Al I. The transitions are also arranged here in four groups. Following the conclusions by Pehlivan Rhodin et al. (2017) and Pehlivan Rhodin (2018), the transitions involving any of the $3s7p\ ^{1,3}$P states have been excluded from this analysis. The discrepancies between the length and velocity forms for transitions including the $3s7p\ ^{1,3}$P states are consistently large, and thus the computed transition rates are not trustworthy. We note that overall the average uncertainty, as well as the value that includes 75% of the data, appear to be smaller, for each group of transitions, than the predicted values in Al I. Nevertheless, the maximum values of the uncertainties for the last two groups are larger in comparison to Al I. This is due to some transitions involving $3p3d\ ^3$F as the upper level. The strong mixing between the $3p3d\ ^3$F and the $3s6f\ ^3$F levels results in strong cancellation effects. Such effects often hamper the accuracy of the computed transition data and result in large discrepancies between the length and velocity forms.

In Table 7, current RCI theoretical transition rates are compared with the values from the MCHF-BP calculations by Froese Fischer et al. (2006) and, whenever available, results from the B-spline configuration interaction (BSCI) calculations by Chang & Fang (1995). For the majority of the transitions, there is an excellent agreement between the RCI and MCHF-BP values with the relative difference being less than 1%. Some of the largest discrepancies are observed for the $3s3d, 3p^2\ ^1D \rightarrow 3s3p\ ^{1,3}P^o$ transitions. According to Froese Fischer et al. (2006), correlation is extremely important for transitions from such ^{1}D states. In the MCHF-BP calculations, all three types of correlation, i.e. VV, CV, and CC, have been accounted for; however, the CSF expansions obtained from SD-substitutions are not as large as in the present calculations and the LS-composition of the configurations might not be predicted as accurately. Hence, the evaluation of line strengths for transitions involving ^{1}D states and in turn the computation of transition rates involving these states will be affected. Computed transition rates using the BSCI approach are provided for transitions that involve only singlet states. The BSCI calculations do not account for the relativistic interaction and no separate values are given for the different fine-structure components of triplet states. For the $3p^2\ ^1D \rightarrow 3s3p\ ^1P^o$ transition, the discrepancy between the RCI and BSCI values is also quite large. On the other hand, for the $3s3d\ ^1D \rightarrow 3s3p\ ^1P^o$ transition, the BSCI result is in perfect agreement with the present $A_{\rm RCI}$ value. The agreement between the current RCI and BSCI transition rates exhibits a broad variation. The advantage of the BSCI approach is that it takes into account the effect of the positive-energy continuum orbitals in an explicit manner. Nevertheless, the parametrized model potential that is being used in the work by Chang & Fang (1995) is not sufficient to describe states that are strongly mixed. Finally, we note the discrepancy for the $3s4p\ ^1P^o \rightarrow 3s^2\ ^1S_0$ transition, which is quite large between the RCI and MCHF-BP values and inexplicably large between the RCI and BSCI values.

In singly ionized aluminium, measurements of transition properties are available only for a few transitions. In Table 7, the available experimental results are compared with the theoretical results from the current RCI calculations, and with the former calculations by Froese Fischer et al. (2006) and Chang & Fang (1995). Transition rates have been experimentally observed for the $3s3p\ ^{1,3}P^o_1 \rightarrow 3s^2\ ^1S_0$ transitions in the works by Kernahan et al. (1979), Smith (1970), Berry et al. (1970) and Head et al. (1976), and by Träbert et al. (1999) and Johnson et al. (1986), respectively. In Table 7, the average value of these works is displayed. The agreement with the current RCI results is fairly good. Nonetheless, the averaged $A_{\rm obs}$ by Träbert et al. (1999) and Johnson et al. (1986) is in better agreement with the value by Froese Fischer et al. (2006). Additionally, Vujnović et al. (2002) provided experimental transition rates for the $3p^2\ ^1D_2 \rightarrow 3s3p\ ^1P_1$ and $3p^2\ ^1D_2 \rightarrow 3s3p\ ^3P_{1,2}$ transitions by measuring relative intensities of spectral lines. These experimental results, however, differ from the theoretical values.

In the last portion of Table 7, current rates for transitions between states with higher energies are compared with the results from the close coupling (CC) calculations by Butler et al. (1993) and the early results from the configuration interaction (CI) calculations by Chang & Wang (1987). The results from the latter two calculations are found to be in very good agreement. Furthermore, the agreement between the RCI results and those from the CC and CI calculations is also very good

Table 7. Comparison between computed and observed transition rates A in s^{-1} for selected transitions in Al II.

Upper	Lower	A_{RCI} [a]	A_{theor} [b,c]	A_{theor} [e,f]	A_{obs} [d,h,g]
$3s3p\ ^3P^o_1$	$3s^2\ ^1S_0$	3.054E+03	3.277E+03[b]		3.30E+03[h]
$3s3p\ ^1P^o_1$	$3s^2\ ^1S_0$	1.404E+09	1.400E+09[b]	1.486E+09[f]	1.45E+09[g]
$3s4s\ ^3S_1$	$3s3p\ ^3P^o_0$	8.612E+07	8.572E+07[b]		
	$3s3p\ ^3P^o_1$	2.555E+08	2.547E+08[b]		
	$3s3p\ ^3P^o_2$	4.173E+08	4.162E+08[b]		
$3s4s\ ^1S_0$	$3s3p\ ^1P^o_1$	3.422E+08	3.455E+08[b]	3.408E+08[f]	
$3p^2\ ^1D_2$	$3s3p\ ^1P^o_1$	2.523E+05	3.804E+05[b]	3.980E+05[f]	1.84E+04[d]
	$3s3p\ ^3P^o_1$	1.790E+04	2.016E+04[b]		0.19E+04[d]
	$3s3p\ ^3P^o_2$	2.827E+04	3.141E+04[b]		0.30E+04[d]
$3p^2\ ^3P_0$	$3s3p\ ^3P^o_1$	1.236E+09	1.235E+09[b]		
$3p^2\ ^3P_1$	$3s3p\ ^3P^o_0$	4.148E+08	4.144E+08[b]		
	$3s3p\ ^3P^o_1$	3.058E+08	3.062E+08[b]		
	$3s3p\ ^3P^o_2$	5.170E+08	5.167E+08[b]		
$3p^2\ ^3P_2$	$3s3p\ ^3P^o_1$	3.145E+08	3.144E+08[b]		
	$3s3p\ ^3P^o_2$	9.264E+08	9.272E+08[b]		
$3p^2\ ^1S_0$	$3s3p\ ^1P^o_1$	1.020E+09	6.738E+08[b]		
	$3s3p\ ^3P^o_1$	5.021E+08	3.399E+07[b]		
$3s3d\ ^3D_2$	$3s3p\ ^3P^o_1$	8.977E+08	9.072E+08[b]		
	$3s3p\ ^3P^o_2$	3.019E+08	3.046E+08[b]		
$3s3d\ ^3D_3$	$3s3p\ ^3P^o_2$	1.197E+09	1.208E+09[b]		
$3s3d\ ^1D_2$	$3s3p\ ^1P^o_1$	1.388E+09	1.429E+09[b]	1.388E+09[f]	
$3s4p\ ^3P^o_0$	$3s4s\ ^3S_1$	5.639E+07	5.705E+07[b]		
	$3s3d\ ^3D_1$	1.556E+07	1.520E+07[b]		
$3s4p\ ^3P^o_1$	$3s4s\ ^3S_1$	5.649E+07	5.724E+07[b]		
	$3s3d\ ^3D_1$	3.905E+06	3.816E+06[b]		
	$3s3d\ ^3D_2$	1.172E+07	1.146E+07[b]		
$3s4p\ ^3P^o_2$	$3s4s\ ^3S_1$	5.683E+07	5.762E+07[b]		
	$3s3d\ ^3D_1$	1.568E+05	1.541E+05[b]		
	$3s3d\ ^3D_2$	2.361E+06	2.312E+06[b]		
	$3s3d\ ^3D_3$	1.319E+07	1.294E+07[b]		
$3s4p\ ^1P^o_1$	$3s^2\ ^1S_0$	1.527E+06	0.981E+06[b]	5.079E+06[f]	
	$3p^2\ ^1D_2$	5.835E+07	5.897E+07[b]	6.307E+07[f]	
	$3s4s\ ^1S_0$	3.109E+07	2.965E+07[b]	3.111E+07[f]	
$3p3d\ ^3F^o_2$	$3s3d\ ^3D_1$	2.956E+08	2.07E+08[c]	2.14E+08[e]	
$3p3d\ ^3F^o_3$	$3s3d\ ^3D_2$	3.174E+08	2.19E+08[c]	2.25E+08[e]	
$3p3d\ ^3F^o_4$	$3s3d\ ^3D_3$	3.794E+08	2.47E+08[c]	2.54E+08[e]	
$3s4f\ ^3F^o_2$	$3s3d\ ^3D_1$	1.981E+08	1.97E+08[c]	1.98E+08[e]	
$3s4f\ ^3F^o_3$	$3s3d\ ^3D_2$	2.096E+08	2.09E+08[c]	2.07E+08[e]	
$3s4f\ ^3F^o_4$	$3s3d\ ^3D_3$	2.360E+08	2.35E+08[c]	2.33E+08[e]	
$3s5f\ ^3F^o_2$	$3s3d\ ^3D_1$	2.801E+07	2.40E+07[c]	2.50E+07[e]	
$3s5f\ ^3F^o_4$	$3s3d\ ^3D_3$	3.438E+07	2.85E+07[c]	2.90E+07[e]	
$3s6f\ ^3F^o_2$	$3s3d\ ^3D_1$	1.957E+07	2.90E+07[c]	3.10E+07[e]	
	$3s4d\ ^3D_1$	1.116E+07	1.07E+07[c]	1.00E+07[e]	
$3s6f\ ^3F^o_3$	$3s3d\ ^3D_2$	1.910E+07	3.07E+07[c]	3.30E+07[e]	
	$3s4d\ ^3D_2$	1.200E+07	1.14E+07[c]	1.10E+07[e]	
$3s6f\ ^3F^o_4$	$3s3d\ ^3D_3$	1.920E+07	3.46E+07[c]	3.70E+07[e]	
	$3s4d\ ^3D_3$	1.367E+07	1.28E+07[c]	1.20E+07[e]	

Notes. The present values from the RCI calculations are given in Col. 3. In the next two columns, theoretical values from former MCHF-BP, close coupling (CC), configuration interaction (CI), and B-spline configuration interaction (BSCI) calculations are given. The last column contains the results from experimental observations. All theoretical transition rates are presented in length form.

References. [(a)]Present calculations; [(b)]Froese Fischer et al. (2006); [(c)]Butler et al. (1993); [(d)]Vujnović et al. (2002); [(e)]Chang & Wang (1987); [(f)]Chang & Fang (1995); [(g)]Kernahan et al. (1979), Smith (1970), Berry et al. (1970), Head et al. (1976); [(h)]Träbert et al. (1999), Johnson et al. (1986).

for the $3s4f\ ^3F \rightarrow 3s3d\ ^3D$ transitions and fairly good for the $3s5f\ ^3F \rightarrow 3s3d\ ^3D$ transitions. On the other hand, for the 3p3d, $3s6f\ ^3F \rightarrow 3s3d\ ^3D$ transitions, the observed discrepancy between the current RCI values and those from the two previous calculations is substantial. This outcome indicates that the calculations by Butler et al. (1993) and Chang & Wang (1987) are insufficient to properly account for correlation and further emphasizes the quality of the present work.

In the same way as for Al I, the lifetimes of Al II excited states were also estimated based on the computed E1 transitions. In Table A.2, both length τ_l and velocity τ_v forms of the currently computed lifetimes are displayed. As already mentioned, the agreement between these two forms serves as an indication of the quality of the results. The average relative difference between the two forms is ∼2%. The largest discrepancies are observed between the length and velocity gauges of the singlet $3p^2\ ^1D$ state, and between the singlet and triplet $3s7p\ ^{1,3}P$ states. The highest computed levels in the calculations of Al II correspond to configuration states with orbitals up to $n = 7$, such as 3s7p. Similarly to the conclusions for the lifetimes of Al I, better agreement between the length and velocity forms of the $3s7p\ ^{1,3}P$ states could probably be obtained by including 3snl configurations with $n > 7$ in the MR.

In Table A.2, the lifetimes from the current RCI calculations are compared with results from previous MCHF-BP and BSCI calculations by Froese Fischer et al. (2006) and Chang & Fang (1995), respectively. Except for the lifetimes of the triplet $3s3p\ ^3P^o_1$ and singlet $3p^2\ ^1D_2$ states, the agreement between the RCI and MCHF-BP calculations is very good. Furthermore, the overall agreement between the RCI and BSCI calculations is sufficiently good. Despite the poor agreement between the RCI and BSCI values for the $3p^2\ ^1D_2$ and $3s7p\ ^{1,3}P$ states, for the rest of the states the discrepancies are small. The BSCI results are more extended. However, no separate values are provided for the different LSJ-components of the triplet states and the average lifetime is presented for them instead.

In Table A.2, the theoretical lifetimes are also compared with available measurements. The measured lifetime of the $3s3p\ ^3P^o_1$ state by Träbert et al. (1999) and Johnson et al. (1986) agrees remarkably well with the calculated value by Froese Fischer et al. (2006). The agreement with the current results is fairly good too. The lifetime of the $3s3p\ ^1P^o_1$ state measured by Kernahan et al. (1979), Head et al. (1976), Berry et al. (1970), and Smith (1970) is well represented by all theoretical values. On the other hand, the results from the measurements of the $3snf\ ^3F$ states by Andersen et al. (1971) differ substantially from the theoretical RCI values. For the $3snf\ ^3F$ Rydberg series, only theoretical lifetimes using the current MCDHF and RCI approach are available. Given the large uncertainties associated with early beam-foil measurements, the discrepancies between theoretical and experimental values are in some way expected. The only exception is the lifetime of the $3s5f\ ^3F$ state, which is in rather good agreement with the RCI values. In the experiments by Andersen et al. (1971) the different fine-structure components have not been separated and a single value is provided for all three different LSJ-levels.

5. Summary and conclusions

In the present work, updated and extended transition data and lifetimes are made available for both Al I and Al II. The computations of transition properties in these two systems are challenging mainly due to the strong two-electron interaction between the $3s3d\ ^1D$ and $3p^2\ ^1D$ states, which dominates the lowest part of their spectra. Thus, some of the states are strongly mixed and highly correlated wave functions are needed to accurately predict their LS-composition. We are confident that in this work enough correlation has been included to affirm the reliability of the results. The predicted excitation energies are in excellent agreement with the experimental data provided by the NIST database, which is a good indicator of the quality of the produced transition data and lifetimes.

We have performed an extensive comparison of the computed transition rates and lifetimes with the most recent theoretical and experimental results. There is a significant improvement in accuracy, in particular for the more complex system of neutral Al I. The computed lifetimes of Al I are in very good agreement with the measured lifetimes in high-precision laser spectroscopy experiments. The same holds for the measured lifetimes of Al II in ion storage rings. The present calculations are extended to higher energies and many of the computed transitions fall in the infrared spectral region. The new generation of telescopes are designed for this region and these transition data are of high importance. The objective of this work is to make available atomic data that could be used to improve the interpretation of abundances in stars. Lists of trustworthy elemental abundances will permit the tracing of stellar evolution, as well as the formation and chemical evolution of the Milky Way.

The agreement between the length and velocity gauges of the transition operator serves as a criterion for the quality of the transition data and for the lifetimes. For most of the strong transitions in both Al I and Al II, the agreement between the two gauges is very good. For transitions involving states with the highest n quantum number for the s and p symmetries, we observe that the agreement between the length and velocity forms is not as good. This becomes more evident when estimating lifetimes of excited levels that are associated with those transitions.

Acknowledgements. The authors have been supported by the Swedish Research Council (VR) under contract 2015-04842. The authors acknowledge H. Hartman, Malmö University, and H. Jönsson, Lund University, for discussions.

References

Adibekyan, V. Z., Sousa, S. G., Santos, N. C., et al. 2012, A&A, 545, A32
Andersen, T., Roberts, J. R., & Sørensen, G. 1971, Phys. Scr., 4, 52
Bensby, T., Feltzing, S., & Oey, M. S. 2014, A&A, 562, A71
Berry, H. G., Bromander, J., & Buchta, R. 1970, Phys. Scr., 1, 181
Butler, K., Mendoza, C., & Zeippen, C. 1993, J. Phys. B, 26, 4409
Buurman, E., & Dönszelmann, A. 1990, A&A, 227, 289
Buurman, E., Dönszelmann, A., Hansen, J. E., & Snoek, C. 1986, A&A, 164, 224
Carretta, E., Bragaglia, A., Gratton, R. G., et al. 2010, A&A, 516, A55
Chang, T. N., & Fang, T. K. 1995, Phys. Rev. A, 52, 2638
Chang, T. N., & Wang, R. 1987, Phys. Rev. A, 36, 3535
Clayton, D. D. 2003, Handbook of Isotopes in the Cosmos: Hydrogen to Gallium (Cambridge: Cambridge University Press)
Davidson, M. D., Volten, H., & Dönszelmann, A. 1990, A&A, 238, 452
Dyall, K. G., Grant, I. P., Johnson, C., Parpia, F. A., & Plummer, E. P. 1989, Comput. Phys. Commun., 55, 425
Ekman, J., Godefroid, M., & Hartman, H. 2014, Atoms, 2, 215
Froese Fischer, C. 2009, Phys. Scr., T134, 014019
Froese Fischer, C., Tachiev, G., & Irimia, A. 2006, At. Data Nucl. Data Tables, 92, 607
Froese Fischer, C., Godefroid, M., Brage, T., Jönsson, P., & Gaigalas, G. 2016, J. Phys. B: At. Mol. Opt. Phys., 49, 182004
Gaigalas, G., Rudzikas, Z., & Froese Fischer, C. 1997, J. Phys. B: At. Mol. Opt. Phys., 30, 3747
Gaigalas, G., Fritzsche, S., & Grant, I. P. 2001, Comput. Phys. Commun., 139, 263
Gaigalas, G., Zalandauskas, T., & Rudzikas, Z. 2003, At. Data Nucl. Data Tables, 84, 99
Gaigalas, G., Zalandauskas, T., & Fritzsche, S. 2004, Comput. Phys. Commun., 157, 239
Gaigalas, G., Froese Fischer, C., Rynkun, P., & Jönsson, P. 2017, Atoms, 5, 6
Gehren, T., Liang, Y. C., Shi, J. R., Zhang, H. W., & Zhao, G. 2004, A&A, 413, 1045
Gehren, T., Shi, J. R., Zhang, H. W., Zhao, G., & Korn, A. J. 2006, A&A, 451, 1065
Grant, I. P. 1974, J. Phys. B, 7, 1458

Grant, I. P. 2007, Relativistic Quantum Theory of Atoms and Molecules (New York: Springer)
Head, M. E. M., Head, C. E., & Lawrence, J. N. 1976, in Atomic Structure and Lifetimes, eds. F. A. Sellin, & D. J. Pegg (NY: Plenum), 147
Hibbert, A. 1989, Phys. Scr., 39, 574
Jönsson, G., & Lundberg, H. 1983, Z. Phys. A, 313, 151
Johnson, B. C., Smith, P. L., & Parkinson, W. H. 1986, ApJ, 308, 1013
Jönsson, G., Kröll, S., Persson, A., & Svanberg, S. 1984, Phys. Rev. A, 30, 2429
Jönsson, P., Gaigalas, G., Bieroń, J., Froese Fischer, C., & Grant, I. P. 2013, Phys. Commun., 184, 2197
Kelleher, D. E., & Podobedova, L. I. 2008a, J. Phys. Chem. Ref. Data, 37, 709
Kelleher, D. E., & Podobedova, L. I. 2008b, J. Phys. Chem. Ref. Data, 37, 267
Kernahan, J. A., Pinnington, E. H., O'Neill, J. A. M., Brooks, R. L., & Donnely, K. E. 1979, Phys. Scrip., 19, 267
Kramida, A., Ralchenko, Y. u., & Reader, J. NIST ASD Team 2018, NIST Atomic Spectra Database, ver. 5.5.3 (Online), available: https://physics.nist.gov/asd (2018, March 15), National Institute of Standards and Technology, Gaithersburg, MD
Lin, C. D. 1974, ApJ, 187, 385
McKenzie, B. J., Grant, I. P., & Norrington, P. H. 1980, Comput. Phys. Commun., 21, 233
Mendoza, C., Eissner, W., Le Dourneuf, M., & Zeippen, C. J. 1995, J. Phys. B, 28, 3485
Mishenina, T. V., Soubiran, C., Bienaymé, O., et al. 2008, A&A, 489, 923
Nordlander, T., & Lind, K. 2017, A&A, 607, A75
Olsen, J., Roos, B. O., Jorgensen, P., & Jensen, H. J. A. a. 1988, J. Chem. Phys., 89, 2185
Pehlivan Rhodin, A., Hartman, H., Nilsson, H., & Jönsson, P. 2017, A&A, 598, A102
Pehlivan Rhodin, A. 2018, Ph. D. Thesis, Lund Observatory
Reddy, B. E., Lambert, D. L., & Allende Prieto, C. 2006, MNRAS, 367, 1329
Smiljanic, R., Korn, A. J., Bergemann, M., Frasca, A., et al. 2014, A&A, 570, A122
Smiljanic, R., Romano, D., Bragaglia, A., Donati, P., et al. 2016, A&A, 589, A115
Smith, W. H. 1970, NIM, 90, 115
Sturesson, L., Jönsson, P., & Fischer, C. F. 2007, Comput. Phys. Commun., 177, 539
Tayal, S. S., & Hibbert, A. 1984, J. Phys. B, 17, 3835
Taylor, P. R. C. W., Bauschlicher, J., & Langhoff, S. 1988, J. Phys. B, 21, L333
Theodosiou, C. E. 1992, Phys. Rev. A, 45, 7756
Trefftz, E. 1988, J. Phys. B: At. Mol. Opt. Phys., 21, 1761
Träbert, E., Wolf, A., & Linkemann, J. 1999, J. Phys. B, 32, 637
Vujnović, V., Blagoev, K., Fürböck, C., Neger, T., & Jäger, H. 2002, A&A, 338, 704
Weiss, A. W. 1974, Phys. Rev., 9, 1524
Wiese, W. L., Smith, M. W., & Miles, B. M. 1969, NSRDS-NBS, 22, 47
Wiese, W. L., & Martin, G. A. 1980, in Transition Probabilities, Part II, Vol. Natl. Stand. Ref. Data System., (Washington DC), Natl. Bur. Std., 68

Appendix A: Additional tables

Table A.1. Computed excitation energies in cm^{-1} for the 78 lowest states in Al II.

			VV								
Pos.	Conf.	LSJ	$n = 8$	$n = 9$	$n = 10$	$n = 11$	$n = 12$	$n = 13$	CV	E_{obs}[a]	ΔE
1	$3s^2$	$^1S_0$	0	0	0	0	0	0	0	0	0
2	3s 3p	$^3P^o_0$	36 227	36 280	36 298	36 318	36 332	36 335	37 445	37 393	−52
3		$^3P^o_1$	36 286	36 339	36 357	36 377	36 391	36 394	37 503	37 454	−49
4		$^3P^o_2$	36 405	36 459	36 477	36 496	36 511	36 514	37 626	37 578	−48
5		$^1P^o_1$	59 810	59 698	59 617	59 619	59 606	59 602	59 982	59 852	−130
6	$3p^2$	$^1D_2$	83 542	83 596	83 620	83 641	83 657	83 660	85 692	85 481	−211
7	3s 4s	$^3S_1$	89 965	90 028	90 059	90 082	90 099	90 102	91 425	91 275	−150
8	$3p^2$	$^3P_0$	92 679	92 709	92 716	92 736	92 750	92 752	94 211	94 085	−126
9		$^3P_1$	92 739	92 769	92 776	92 795	92 809	92 812	94 264	94 147	−117
10		$^3P_2$	92 855	92 885	92 892	92 912	92 926	92 928	94 375	94 269	−106
11	3s 4s	$^1S_0$	94 003	94 057	94 084	94 101	94 111	94 114	95 543	95 351	−192
12	3s 3d	$^3D_2$	94 262	94 243	94 241	94 262	94 278	94 280	95 791	95 549	−242
13		$^3D_1$	94 261	94 243	94 242	94 263	94 279	94 281	95 794	95 551	−243
14		$^3D_3$	94 263	94 242	94 239	94 261	94 276	94 279	95 804	95 551	−253
15	3s 4p	$^3P^o_0$	103 935	104 003	104 030	104 053	104 070	104 073	105 582	105 428	−154
16		$^3P^o_1$	103 948	104 017	104 044	104 067	104 084	104 087	105 594	105 442	−152
17		$^3P^o_2$	103 976	104 045	104 073	104 095	104 112	104 115	105 623	105 471	−152
18		$^1P^o_1$	105 597	105 643	105 655	105 673	105 683	105 685	107 132	106 921	−211
19	3s 3d	$^1D_2$	109 010	108 919	108 897	108 910	108 918	108 918	110 330	110 090	−240
20	$3p^2$	$^1S_0$	111 100	110 804	110 659	110 643	110 618	110 608	112 086	111 637	−449
21	3s 5s	$^3S_1$	118 564	118 632	118 661	118 685	118 702	118 705	120 259	120 093	−166
22		$^1S_0$	119 807	119 878	119 908	119 931	119 946	119 948	121 544	121 367	−177
23	3s 4d	$^3D_2$	120 013	120 034	120 045	120 068	120 085	120 088	121 684	121 484	−200
24		$^3D_1$	120 013	120 034	120 046	120 068	120 085	120 088	121 685	121 484	−201
25		$^3D_3$	120 014	120 034	120 045	120 068	120 084	120 087	121 688	121 484	−204
26	3s 4f	$^3F^o_2$	121 657	121 739	121 772	121 797	121 815	121 818	123 606	123 418	−188
27		$^3F^o_3$	121 659	121 742	121 775	121 799	121 817	121 820	123 608	123 420	−188
28		$^3F^o_4$	121 663	121 745	121 778	121 802	121 820	121 824	123 612	123 423	−189
29		$^1F^o_3$	121 735	121 818	121 852	121 876	121 894	121 898	123 657	123 471	−186
30	3s 4d	$^1D_2$	123 606	123 489	123 461	123 473	123 482	123 483	125 049	124 794	−255
31	3s 5p	$^3P^o_0$	124 108	124 185	124 212	124 236	124 254	124 257	125 869	125 703	−166
32		$^3P^o_1$	124 114	124 190	124 218	124 242	124 259	124 262	125 874	125 709	−165
33		$^3P^o_2$	124 126	124 203	124 231	124 254	124 272	124 275	125 887	125 722	−165
34		$^1P^o_1$	124 302	124 375	124 401	124 424	124 440	124 443	126 078	125 869	−209
35	3s 6s	$^3S_1$	130 615	130 689	130 716	130 740	130 758	130 761	132 386	132 216	−170

Notes. The energies are given as a function of the increasing active set of orbitals, accounting for VV correlation, where n indicates the maximum principle quantum number of the orbitals included in the active set. In Col. 10, the final energy values are displayed after accounting for CV correlation. The differences ΔE between the final computations and the observed values are shown in the last column. The sequence and naming of the configurations and LSJ-levels are in accordance with the final (CV) computed energies. The levels of the singlet and triplet 3s6h ^{1,3}H and the 3p3d ^{1}D level have not yet been observed, and so the ΔE values are not available.

References. [(a)]NIST Atomic Spectra Database 2018 (Kramida et al. 2018).

Table A.1. continued.

			VV								
Pos.	Conf.	*LS J*	$n = 8$	$n = 9$	$n = 10$	$n = 11$	$n = 12$	$n = 13$	CV	E_{obs}[a]	ΔE
36		$^1S_0$	131 160	131 237	131 268	131 291	131 308	131 311	132 953	132 779	−174
37	3s 5d	$^3D_2$	131 265	131 307	131 326	131 348	131 365	131 368	133 013	132 823	−190
38		$^3D_1$	131 265	131 307	131 327	131 348	131 365	131 368	133 013	132 823	−190
39		$^3D_3$	131 266	131 307	131 326	131 347	131 365	131 368	133 017	132 823	−194
40	3s 5f	$^3F^o_2$	131 641	131 712	131 745	131 769	131 787	131 790	133 639	133 438	−201
41		$^3F^o_3$	131 647	131 718	131 751	131 776	131 794	131 797	133 644	133 443	−201
42		$^3F^o_4$	131 655	131 727	131 760	131 785	131 803	131 806	133 654	133 450	−204
43		$^1F^o_3$	131 968	132 048	132 082	132 106	132 124	132 128	133 866	133 682	−184
44	3s 5d	$^1D_2$	132 490	132 447	132 445	132 460	132 474	132 476	134 143	133 916	−227
45	3s 5g	$^3G_3$	132 487	132 577	132 611	132 636	132 654	132 657	134 359	134 184	−175
46		$^3G_4$	132 487	132 577	132 611	132 636	132 654	132 658	134 360	134 184	−176
47		$^3G_5$	132 487	132 577	132 611	132 636	132 654	132 657	134 360	134 184	−176
48		$^1G_4$	132 487	132 577	132 611	132 636	132 654	132 658	134 360	134 184	−176
49	3s 6p	$^1P^o_1$	133 288	133 366	133 387	133 411	133 428	133 431	135 132	134 919	−213
50		$^3P^o_0$	133 378	133 459	133 485	133 509	133 526	133 530	135 183	135 012	−171
51		$^3P^o_1$	133 381	133 462	133 488	133 512	133 530	133 533	135 186	135 016	−170
52		$^3P^o_2$	133 388	133 468	133 494	133 518	133 536	133 539	135 192	135 022	−170
53	3s 7s	$^3S_1$	136 870	136 949	136 975	136 999	137 014	137 017	138 675	138 500	−175
54	3s 6f	$^3F^o_2$	136 665	136 628	136 655	136 678	136 695	136 698	138 810	138 521	−289
55		$^3F^o_3$	136 684	136 649	136 677	136 699	136 717	136 720	138 829	138 539	−290
56		$^3F^o_4$	136 709	136 677	136 704	136 727	136 745	136 748	138 862	138 562	−300
57	3s 7s	$^1S_0$	137 154	137 236	137 267	137 291	137 307	137 311	138 974	138 801	−173
58	3s 6d	$^3D_2$	137 217	137 273	137 297	137 314	137 331	137 333	139 005	138 815	−190
59		$^3D_1$	137 217	137 273	137 297	137 314	137 331	137 333	139 005	138 815	−190
60		$^3D_3$	137 218	137 273	137 297	137 314	137 331	137 333	139 010	138 815	−195
61	3s 6f	$^1F^o_3$	137 562	137 625	137 657	137 681	137 699	137 702	139 437	139 245	−192
62	3s 6d	$^1D_2$	137 753	137 754	137 767	137 786	137 801	137 803	139 497	139 289	−208
63	3s 6g	$^3G_3$	137 898	137 988	138 022	138 046	138 065	138 067	139 766	139 591	−175
64		$^3G_4$	137 898	137 988	138 022	138 046	138 065	138 068	139 766	139 591	−175
65		$^3G_5$	137 898	137 988	138 022	138 046	138 065	138 067	139 766	139 591	−175
66		$^1G_4$	137 898	137 988	138 022	138 047	138 065	138 068	139 766	139 591	−175
67	3s 6h	$^3H^o_4$	137 965	138 043	138 079	138 103	138 121	138 125	139 817		
68		$^3H^o_5$	137 965	138 043	138 079	138 103	138 121	138 125	139 817		
69		$^1H^o_5$	137 965	138 043	138 079	138 103	138 121	138 125	139 817		
70		$^3H^o_6$	137 965	138 043	138 079	138 103	138 121	138 125	139 817		
71	3s 7p	$^1P^o_1$	138 286	138 364	138 360	138 384	138 401	138 402	140 148	139 919	−229
72		$^3P^o_0$	138 439	138 522	138 545	138 569	138 587	138 589	140 266	140 090	−176
73		$^3P^o_1$	138 441	138 524	138 547	138 571	138 589	138 591	140 268	140 092	−176
74		$^3P^o_2$	138 445	138 529	138 552	138 575	138 593	138 595	140 272	140 096	−176
75	3p 3d	$^3F^o_2$	136 665	136 628	136 655	136 678	136 695	139 291	141 615	141 085	−531
76		$^3F^o_3$	136 684	136 649	136 677	136 699	136 717	139 311	141 665	141 110	−555
77		$^3F^o_4$	136 709	136 677	136 704	136 727	136 745	139 338	141 768	141 143	−625
78	3p 3d	$^1D^o_2$	140 333	140 372	140 385	140 408	140 425	140 428	142 964		

Table A.2. Comparison between computed and observed lifetimes τ in seconds for 75 excited states in Al II.

			RCI[a]		MCHF-BP[b]	BSCI[c]	Expt.[d,e,f]
Pos.	Conf.	*LS J*	τ_l	τ_v	τ_l		$\tau_{\rm obs}$
1	3s3p	$^3P^o_1$	3.274E-04	2.965E-04	3.051E-04		3.02 (2) E-04[e]
2		$^1P^o_1$	7.120E-10	7.089E-10	7.141E-10	6.70 E-10	6.90(13)E-10[d]
3	$3p^2$	$^1D_2$	3.351E-06	2.630E-06	2.270E-06	2.51 E-06	
4	3s4s	$^3S_1$	1.318E-09	1.325E-09	1.322E-09	1.32 E-09	
5	$3p^2$	$^3P_0$	8.091E-10	8.032E-10	8.098E-10		
6		$^3P_1$	8.081E-10	8.023E-10	8.082E-10		
7		$^3P_2$	8.059E-10	8.000E-10	8.054E-10		
8	3s4s	$^1S_0$	2.921E-09	2.922E-09	2.893E-09	2.93 E-09	
9	3s3d	$^3D_2$	8.337E-10	8.346E-10	8.252E-10	8.00 E-10	
10		$^3D_1$	8.319E-10	8.328E-10	8.233E-10	8.00 E-10	
11		$^3D_3$	8.358E-10	8.357E-10	8.277E-10	8.00 E-10	
12	3s4p	$^3P^o_0$	1.390E-08	1.394E-08	1.384E-08	1.403E-08	
13		$^3P^o_1$	1.386E-08	1.391E-08	1.379E-08	1.403E-08	
14		$^3P^o_2$	1.379E-08	1.384E-08	1.369E-08	1.403E-08	
15		$^1P^o_1$	1.099E-08	1.113E-08	1.116E-08	1.007E-08	
16	3s3d	$^1D_2$	7.204E-10	7.192E-10	6.994E-10	7.20 E-10	
17	$3p^2$	$^1S_0$	9.804E-10	9.758E-10	9.720E-10	9.50 E-10	
18	3s5s	$^3S_1$	2.767E-09	2.785E-09		2.78 E-09	
19		$^1S_0$	4.059E-09	4.055E-09		4.33 E-09	
20	3s4d	$^3D_2$	3.862E-09	3.872E-09		3.71 E-09	
21		$^3D_1$	3.850E-09	3.860E-09		3.71 E-09	
22		$^3D_3$	3.880E-09	3.889E-09		3.71 E-09	
23	3s4f	$^3F^o_2$	4.235E-09	4.254E-09			6.4 (5)E-09[f]
24		$^3F^o_3$	4.230E-09	4.248E-09			6.4 (5)E-09[f]
25		$^3F^o_4$	4.230E-09	4.256E-09			6.4 (5)E-09[f]
26		$^1F^o_3$	3.428E-09	3.438E-09			
27	3s4d	$^1D_2$	1.366E-09	1.368E-09		1.31 E-09	
28	3s5p	$^3P^o_0$	4.903E-08	4.941E-08		4.928E-08	
29		$^3P^o_1$	4.862E-08	4.899E-08		4.928E-08	
30		$^3P^o_2$	4.850E-08	4.903E-08		4.928E-08	
31		$^1P^o_1$	1.315E-08	1.377E-08		1.263E-08	
32	3s6s	$^3S_1$	5.196E-09	5.242E-09		5.19 E-09	
33		$^1S_0$	7.265E-09	7.254E-09		7.61 E-09	
34	3s5d	$^3D_2$	1.077E-08	1.081E-08		1.03 E-08	
35		$^3D_1$	1.073E-08	1.077E-08		1.03 E-08	

Notes. For the current RCI calculations length τ_l and velocity τ_v forms are both displayed. In Cols. 6 and 7, the predicted lifetimes from MCHF-BP and BSCI calculations are, respectively, given in length form. The last column contains available lifetimes from experimental measurements, together with their uncertainties.

References. [(a)]Present calculations; [(b)]Froese Fischer et al. (2006); [(c)]Chang & Fang (1995); [(d)]Kernahan et al. (1979), Smith (1970), Berry et al. (1970), Head et al. (1976); [(e)]Träbert et al. (1999), Johnson et al. (1986); [(f)]Andersen et al. (1971).

Table A.2. continued.

Pos.	Conf.	$LS\,J$	RCI[a] τ_l	RCI[a] τ_v	MCHF-BP[b] τ_l	BSCI[c]	Expt.[d,e,f] $\tau_{\rm obs}$
36		$^3D_3$	1.085E-08	1.090E-08		1.03 E-08	
37	3s5f	$^3F^o_2$	1.337E-08	1.356E-08			1.4 (2)E-08[f]
38		$^3F^o_3$	1.328E-08	1.348E-08			1.4 (2)E-08[f]
39		$^3F^o_4$	1.320E-08	1.345E-08			1.4 (2)E-08[f]
40		$^1F^o_3$	5.981E-09	6.015E-09			
41	3s5d	$^1D_2$	3.523E-09	3.525E-09		3.37 E-09	
42	3s5g	$^3G_3$	1.389E-08	1.390E-08			
43		$^3G_4$	1.389E-08	1.389E-08			
44		$^3G_5$	1.389E-08	1.390E-08			
45		$^1G_4$	1.383E-08	1.384E-08			
46	3s6p	$^1P^o_1$	1.322E-08	1.425E-08		1.211E-08	
47		$^3P^o_0$	1.147E-07	1.171E-07		1.105E-07	
48		$^3P^o_1$	1.097E-07	1.122E-07		1.105E-07	
49		$^3P^o_2$	1.137E-07	1.173E-07		1.105E-07	
50	3s7s	$^3S_1$	9.039E-09	9.167E-09		8.78 E-09	
51	3s6f	$^3F^o_2$	2.041E-08	2.051E-08			1.5 (1)E-08[f]
52		$^3F^o_3$	2.111E-08	2.125E-08			1.5 (1)E-08[f]
53		$^3F^o_4$	2.222E-08	2.236E-08			1.5 (1)E-08[f]
54	3s7s	$^1S_0$	1.174E-08	1.170E-08			
55	3s6d	$^3D_2$	2.386E-08	2.399E-08		2.234E-08	
56		$^3D_1$	2.376E-08	2.391E-08		2.234E-08	
57		$^3D_3$	2.423E-08	2.445E-08		2.234E-08	
58	3s6f	$^1F^o_3$	9.655E-09	9.720E-09			
59	3s6d	$^1D_2$	7.546E-09	7.518E-09		7.46 E-09	
60	3s6g	$^3G_3$	2.415E-08	2.417E-08			
61		$^3G_4$	2.412E-08	2.413E-08			
62		$^3G_5$	2.417E-08	2.415E-08			
63		$^1G_4$	2.373E-08	2.375E-08			
64	3s6h	$^3H^o_4$	3.753E-08	3.759E-08			
65		$^3H^o_5$	3.753E-08	3.759E-08			
66		$^1H^o_5$	3.753E-08	3.759E-08			
67		$^1H^o_6$	3.753E-08	3.759E-08			
68	3s7p	$^1P^o_1$	1.238E-08	1.450E-08		1.081E-08	
69		$^3P^o_0$	1.904E-07	2.090E-07		1.608E-07	
70		$^3P^o_1$	1.897E-07	2.078E-07		1.608E-07	
71		$^3P^o_2$	1.865E-07	2.148E-07		1.608E-07	
72	3p3d	$^3F^o_2$	2.769E-09	2.735E-09			3.5 (3)E-09[f]
73		$^3F^o_3$	2.736E-09	2.701E-09			3.5 (3)E-09[f]
74		$^3F^o_4$	2.586E-09	2.539E-09			3.5 (3)E-09[f]
75		$^1D^o_2$	8.207E-10	8.198E-10			